Fluorescence Image Segmentation by using Digitally Reconstructed Fluorescence Images

Clemens Blumer[1], Cyprien Vivien[2], Thomas G. Oertner[2], Thomas Vetter[1]

[1]Department of Mathematics and Computer Science, University of Basel, Switzerland
{clemens.blumer, thomas.vetter}@unibas.ch
[2]Friedrich Miescher Institute for Biomedical Research, Basel, Switzerland
{cyprien.vivien, thomas.oertner}@fmi.ch

***Abstract*— In biological experiments fluorescence imaging is used to image living and stimulated neurons. But the analysis of fluorescence images is a difficult task. It is not possible to conclude the shape of an object from fluorescence images alone. Therefore, it is not feasible to get good manual segmented nor ground truth data from fluorescence images. Supervised learning approaches are not possible without training data. To overcome this issues we propose to synthesize fluorescence images and call them 'Digitally Reconstructed Fluorescence Images' (DRFI). We propose how DRFIs are computed with data from 'Serial Block-Face Scanning Electron Microscopy' (SBFS-EM). As novelty, we use DRFIs to learn a distribution model of dendrite intensities and apply it to classify pixels into spine and non-spine pixels. By using DRFIs as test data we also have the ground truth of spine and non-spine pixels and can validate the results. With DRFIs supervised learning of fluorescence images is feasible.**

I. Introduction

In the biological field the bottleneck moved from data generation to data analysis. Neurobiologists heavily use microscopy to investigate how neurons communicate. Thanks to fluorescence imaging (neurons are filled with fluorescent dyes as a volume marker) it becomes possible to image live cells over time with a high resolution resolving dendrites and spines (Fig. 1 shows schematic neurons).

Fluorescence images are intensity images. In the sample, proteins are excited and emit photons that are counted. No optical mapping of an object to its fluorescence image exists (this means, there is no direct reflection of light). The emission and the point spread function (PSF) of e.g. 2-photon imaging is large and blurry. The resulting images lack of edges respectively surfaces. It is not possible to conclude the object shape from the fluorescence image. 3D fluorescence images are highly anisotropicly blurred. Therefore, the use of classical 3D image analysis is not feasible. Even for experienced biologists it is very challenging to segment objects or structures in fluorescence images. Fluorescence images are difficult to be analyzed automatically. The evaluation of results is very ambitious because there does not exist real ground truth data. Automated image analysis using supervised learning requires training data. In the domain of fluorescence images the generation of training data is very difficult. In contrast, the manual reconstruction of specially prepared, fixed dendrites in electron microscopy (EM) images is possible. These reconstructions have the correct geometrical properties of the dendrites. It is feasible to (manually) identify different structures (e.g. spines) in the reconstructions. This motivates to compute training data from EM reconstructions.

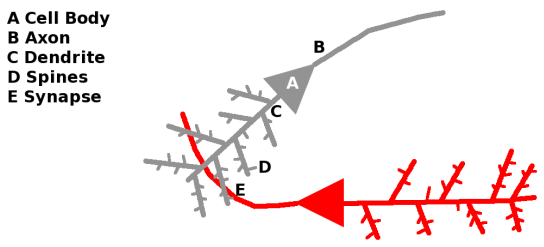

Fig. 1. Signals are sent from cell to cell over axons (*B*) to dendrites (*C*). The connection between axons and dendrite is often located at spines (*D*) and is called synapse (*E*).

In our approach we combine 2-photon imaging and electron microscopy and transfer *a-priori* knowledge from EM reconstructions to the 2-photon imaging modality. The conjunction of the two modalities is realized by computing synthetic fluorescence images that we call 'Digitally Reconstructed Fluorescence Images' (DRFI). This enables automated fluorescence image analysis algorithms based on supervised learning.

Furthermore, EM reconstructions and DRFIs provide the possibility to study dendrites and its fluorescence images in different aspects. It is possible to visualize the effect of enclosed structures (e.g. mitochondria) on imaging and how different spines are represented in fluorescence images. Therefore, beside the computation of the statistical variability of the fluorescence response also different (biologically inspired) questions can be studied.

In our studies we focus on the classification into spine and non-spine voxels in fluorescence images. Different approaches exist but none of them uses supervised learning. Many approaches are based on the use of a full skeleton or backbone ([1], [2], [3], [4], [5]) or use the skeleton represented in a different way, e.g. Zhang et al. [6] use vector flows. Shi et al. [7] use the center line to compute a surface. Other approaches like Rodriguez et al. [8] use local threshold methods. We propose a novel approach and model fluorescence intensity of dendrites. Therefore, we propose how a statistical model for fluorescence images can be computed and overcomes the drawbacks of fluorescence images. In the application we model dendrites and segmentations by using Principal Component Analysis (PCA).

Section II introduces the raw data generation. In section III we describe how DRFIs are computed. In section IV we explain the knowledge transfer, a 2D model and its application and in section V we discuss our approach.

II. Raw Data Generation

We image neurons and are interested in dendrites and spines. Dendrites have the size of some μm. We can image with high magnification such that fine structures like spines are visible. Many spines are visible by 2-photon imaging but it is difficult to conclude the geometrical shape from fluorescence images. Therefore, we use electron microscopy and DRFIs.

Since years electron microscopy is used to image small structures like spines in high resolution. Classical electron microscopes like Transmission Electron Microscopy have the disadvantage that the image stack must be aligned and corrected for distortion. In 2004 Denk and Horstmann [9] presented the 'Serial Block-Face Scanning Electron Microscopy' (SBFS-EM). The data does not require an alignment. Image analysis can be done without preprocessing. By the preparation the tissue and neurons are fixed (not possible to do time-lapse imaging). The samples get trimmed to a few hundred μm and are then ready for imaging (for more details about preparations and SBFS-EM in general see [9]).

We imaged with 2-photon imaging and SBFS-EM the same piece of dendrite. This enables us to visually compare the DRFIs with imaged fluorescence images. By a special preparation one cell becomes distinguishable (labeled) from background in SBFS-EM. Then we can easily reconstruct the dendrite of interest (see III-A).

III. Digitally Reconstructed Fluorescence Images (DRFI)

Our data set resolves fine structures like spines in all details in the SBFS-EM modality. But live neurons can only be imaged with fluorescence imaging. It is time consuming and not trivial to acquire both data sets from the same piece of dendrite. We would like to analyze only fluorescence images. Therefore, the knowledge about structures and segmentations must be transferred from the SBFS-EM to the 2-photon imaging modality. We use synthetic fluorescence images to transfer *a-priori* knowledge.

The goal of the DRFI approach is to model information in the 2-photon imaging modality that is very difficult to detect in fluorescence images directly but easily in SBFS-EM data (like e.g. spines and its segmentation).

A. Manual Dendrite Reconstruction in SBFS-EM

Data from the SBFS-EM is used without any previous alignment nor distortion correction. An experienced biologist manually thresholds the data to a binary image. The largest connected object is kept and all others (background noise) are removed. This first reconstruction has enclosed structures which can be divided into artifacts and mitochondria. The artifacts are regions where the labeling failed (in Fig. 2 D an artifact is highlighted with an "X"). The special labeling does not stain mitochondria. To correct the enclosed structures

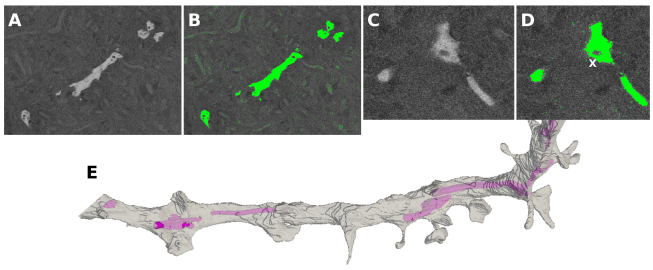

Fig. 2. A,C) Two examples of raw data of SBFS-EM. B,D) Examples with overlaid segmentation (an enclosed structure is at "X"). E) 3D EM reconstruction with visualized mitochondria (*pink*).

all of them are filled and mitochondria volumes are subtracted from the reconstruction. This yields to correct reconstructions of dendrites which exclude mitochondria. This is important because in 2-photon imaging mitochondria is not fluorescent. Fig. 2 shows the raw data and the reconstruction of the dendrite with visualized mitochondria (*E*).

B. Point Spread Function of Fluorescence Images

The response of an imaging system to a point source is called point spread function (PSF). In many imaging systems the spatial extension of the PSF is negligible. But not in 2-photon imaging and similar microscopes. These imaging systems have a large PSF. Furthermore, the PSF is elongated along the optical axis (laser- or z-direction). The PSF can be measured or synthetically approximated. We use a synthetic PSF. This enables us to compute new data (and so new models) for any possible microscope configuration.

Zhang et al. [10] show that a 3D Gaussian distribution approximates the PSF quite accurate:

$$\mathrm{PSF}(x,y,z) = g_{\sigma_p,\sigma_z}(x,y,z) = \exp\left(-\frac{x^2+y^2}{2\sigma_p^2} - \frac{z^2}{2\sigma_z^2}\right) \tag{1}$$

where σ_p is the standard deviation in x,y-direction (plane), σ_z in z-direction and x, y, z is the position relative to the center of the PSF.

Furthermore, Zipfel et al. [11] show a dependency between the $1/e$ width ω_p and ω_z. It is valid that

$$\sigma = \frac{\mathrm{FWHM}}{2\sqrt{2\ln 2}} = \frac{2\sqrt{\ln 2}\omega}{2\sqrt{2\ln 2}} = \frac{\omega}{\sqrt{2}} \tag{2}$$

where FWHM is the full width at half maximum. Therefore, we get for the standard deviations

$$\sigma_p = \begin{cases} \frac{0.320\lambda}{2\mathrm{NA}} & \text{if NA} \leq 0.7 \\ \frac{0.325\lambda}{2\mathrm{NA}^{0.91}} & \text{else} \end{cases} \tag{3}$$

and

$$\sigma_z = \frac{0.532\lambda}{2\left(n - \sqrt{n^2 - \mathrm{NA}^2}\right)} \tag{4}$$

where NA is the numerical aperture, n is the refraction index and λ is the wave length of the laser. The constants are given by Zipfel et al. [11].

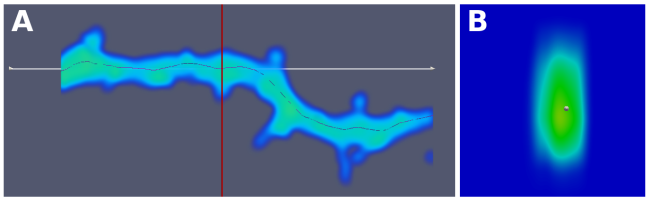

Fig. 3. A) Volume rendering of DRFI with overlaid backbone, visualized backbone-orthogonal plane (*red line*) and normal of the plane (*arrow*). B) Backbone-orthogonal slice extracted from DRFI.

C. Computing Digitally Reconstructed Fluorescence Images

The EM reconstruction is the correct geometrical shape of the objects (dendrites). We assume a homogeneous filled neuron and exclude mitochondria volume. Given the synthetic PSF it is known how every object point is mapped to the 2-photon imaging modality. A convolution of the shape with the PSF gives the DRFI

$$F_d(i,j,k) = R_d(i,j,k) * \mathrm{PSF}_{\mathrm{NA},\lambda,n}(x,y,z) \tag{5}$$

where $R_d(i,j,k)$ is the binary image of the reconstruction. Both images must be sampled at the same rate. This is achieved by resampling or computing the PSF with the required sampling frequency.

IV. Application

In the application we use the computed data to build a PCA model to classify pixels into spine or non-spine. To simplify the classification the model is trained on 2D data extracted from the 3D images.

Dendrites can be illustrated with central curves, also known as backbone. This backbone is the elongation of the dendrite in space. We use 2D images orthogonal to the (manually generated) backbone (see Fig. 3).

Finally, for any 2D backbone-orthogonal slice image a prediction of spines can be done. As *a-priori* knowledge we use DRFIs of dendrites and spine segmentations which are computed like presented in section III. We use DRFI test data. This enables us to validate the results on pixel level. Therefore, the advantages and disadvantages of our approach can be studied in all details. Also some first 2-photon imaging data is analyzed.

Fig. 4 shows the process pipeline. Offline, the training data is computed from the reconstructions and a synthetic PSF in 3D. From the training data then also offline the PCA models are computed. In the testing phase online the 3D fluorescence image (every backbone-orthogonal slice) is approximated with the dendrite model and from this the approximation for the spine probability model is computed. With the parameters for the spine probability model a segmentation of spines in the 3D space is computed. In the following sections the computation and combination of the 2D models is introduced and detailed results for synthetic 3D test data in backbone-orthogonal slices presented. Furthermore, we show some first results on a 3D fluorescence image from 2-photon microscopy where the prediction results are transferred from the backbone-orthogonal slices to the 3D space.

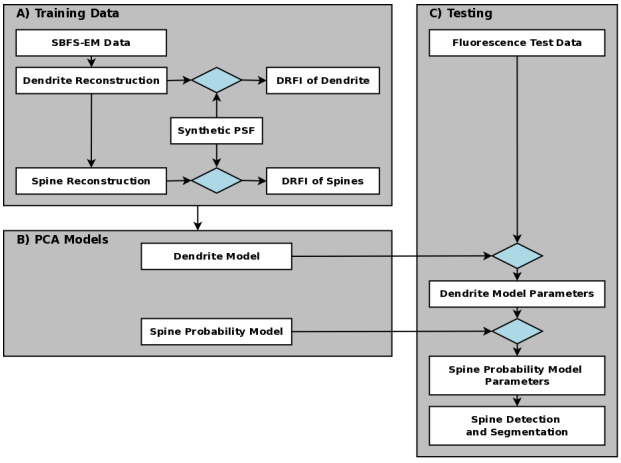

Fig. 4. A) Offline computation of training data. B) Offline Computation of the PCA models. C) Testing Pipeline: For test data the parameters of the dendrite model are computed. Then the parameters for the spine probability model are estimated. Using these parameters the spines are detected and segmented.

A. Transfer of a-priori Knowledge

In EM reconstructions spines and other structures are detectable. The goal of the knowledge transfer is to transfer this information to fluorescence images. Given an EM reconstruction $R_d(i,j,k)$ of the dendrite (including spines) and a manual segmentation $R_s(i,j,k)$ of its spines we can compute the DRFI $F_d(i,j,k)$ of the dendrite including spines reconstruction and a fluorescence image $F_s(i,j,k)$ of the spine segmentation. Because both images are computed with the same PSF the probability for every pixel the intensity is from spine is given by:

$$P_s(i,j,k) = \begin{cases} F_s(i,j,k)/F_d(i,j,k) & \text{if } F_d(i,j,k) > 0 \\ 0 & \text{else} \end{cases} \tag{6}$$

This probability map corresponds to a segmentation in fluorescence images and is the knowledge transfer. It is to mention that there is a smooth transition between spine and dendrite pixels. Therefore, for a final segmentation in fluorescence images a threshold (e.g. $> 50\%$ of intensity from spine) must be applied.

B. PCA Model Computation

From DRFI F_d and the probability image P_s backbone-orthogonal slices $F_{d,i}$ and $P_{s,i}$ with $i = \{1,2,\dots n\}$ are extracted. The slices are scaled. The scaling is per axis (x/y- and z-axis) to compensate the elongated PSF. The intensity is normalized to $\{0,1\}$. Then we compute a dendrite model $\mathrm{PCA}(F_{d,i})$ and a spine probability model $\mathrm{PCA}(P_{s,i})$. The computation for both PCA models is the same and we present it for $\mathrm{PCA}(F_{d,i})$.

First we compute the mean of all n examples as

$$\mu_d = \frac{1}{n}\sum_{i=1}^{n} F_{d,i} \tag{7}$$

and construct the mean-free data matrix:

$$X_d = [F_{d,1} - \mu_d \dots F_{d,n} - \mu_d] \tag{8}$$

Then we do a singular value decomposition of matrix X_d:

$$X_d = U_d D_d V_d^T \tag{9}$$

An arbitrary slice s_d can be written as

$$s_d = \mu_d + U_d \alpha_d \tag{10}$$

where α_d are the *PCA-coefficients*.

C. PCA Model Combination and Prediction

The goal of model combination and prediction is to approximate a test slice by the *PCA-coefficients* of the dendrite model and compute the *PCA-coefficients* of the spine probability model. This yields the prediction maps $s_{s,i}$.

The dendrite model and the spine probability model are constructed of the same slices. Furthermore, any linear combination of principal components u_k can be expressed as linear combination of the example data and vice versa. We assume that a slice of dendrite respectively spine probabilities can be represented by the same linear combination of examples of dendrite slices respectively spine probability maps. Given the assumption it becomes possible to predict the *PCA-coefficients* of one model by the other one. First we right-multiply eq. (9) with $V_d D_d^{-1}$:

$$X_d V_d D_d^{-1} = U_d \tag{11}$$

$\alpha_d = (\alpha_{d,1}, \ldots, \alpha_{d,\tilde{n}})^T$ and $\beta_d = (\beta_{d,1}, \ldots, \beta_{d,\tilde{n}})^T$ are coefficient vectors. Then

$$\sum_{i=1}^{\tilde{n}} \alpha_{d,i} u_{d,i} = U_d \alpha_d = X_d V_d D_d^{-1} \alpha_d = X_d \beta_d = \sum_{i=1}^{n} \beta_{d,i} x_{d,i} \tag{12}$$

and we have the relations

$$\beta_d = V_d D_d^{-1} \alpha_d \tag{13}$$

and

$$\alpha_d = D_d V_d^T \beta_d \tag{14}$$

Given the assumption above introduced about same linear combinations of examples it is valid that $\beta_s = \beta_d$ and we get

$$\alpha_s = D_s V_s^T V_d D_d^{-1} \alpha_d \tag{15}$$

The prediction map s_s for a 2D dendrite image s_d is given by projecting s_d to the dendrite PCA model using

$$\alpha_d = U_d^T (s_d - \mu_d) \tag{16}$$

and retrieve α_s with eq. (15). Finally, the prediction is:

$$s_s = \mu_s + U_s \alpha_s \tag{17}$$

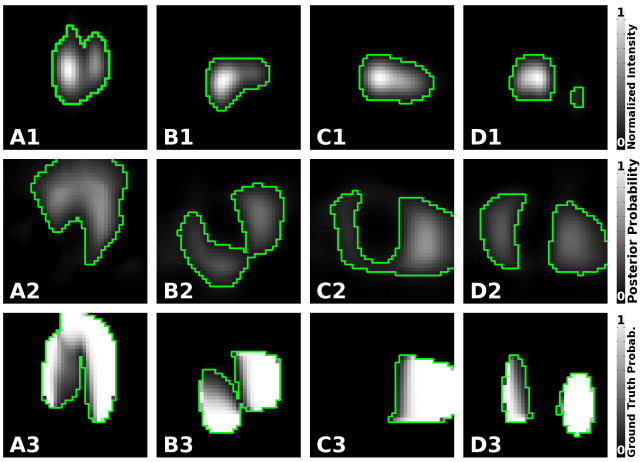

Fig. 5. The *first row* shows examples of DRFI test slices ($F_{d,i}$) and the *second row* the corresponding prediction maps ($s_{s,i}$). The *third row* shows the ground truth probability maps ($P_{s,i}$). The outlines (*green*, 10% of intensity) are marked for better visibility.

D. Results

We used different EM reconstructions for training and testing. First, we present results of synthetic data. This enables us to validate the results with ground truth data. As training data we used an EM reconstruction with 17 spines. The dendrite was rotated along its main axis in 10° steps to compute spines at different orientation relative to the optical axis. Then every $0.02\mu m$ backbone-orthogonal slices (about 20000) with a side length of $4\mu m$ were extracted. The slices were resampled at $0.1\mu m$. From these 20000 slices the PCA model was computed and the first 25 components kept.

Fig. 5 shows results for the test image. From the DRFI of the test dendrite backbone-orthogonal slices $F_{d,i}$ (*first row*) were extracted and the posterior probabilities $s_{s,i}$ computed (*second row*, *third row* shows ground truth probability maps $P_{s,i}$). The posterior probabilities have similar local maxima like the computed ground truth data. With further processing of these posterior probabilities it is possible to conclude from fluorescence images the existence and location of spines and its segmentations.

Furthermore, we computed a binary segmentation of the slices. For the ground truth data we used a threshold of 0.5. The threshold of the posterior probabilities was computed over all slices as $0.5 * \frac{1}{\hat{n}} \sum_i^{\hat{n}} \max(s_{s,i}) \approx 0.23$. This parameter can be tuned. Fig. 6 shows the slices (same examples like in Fig. 5). The binary results for our predictions are shown in the *first row*. The *second row* shows the binary result for the ground truth data. The *third row* shows a classification into correct background (*dark gray*), correct foreground (*white*), missed foreground (*light gray*) and incorrectly as spine classified (*black*) pixels .

In the 544 test slices 92.4% pixels are correctly classified (88.2% background and 4.2% foreground pixels). 4.4% are wrongly classified as spine pixels and 3.2% are missed foreground pixels. Changing the threshold value and further changes improve the results.

Furthermore, the approach was tested with the same piece of

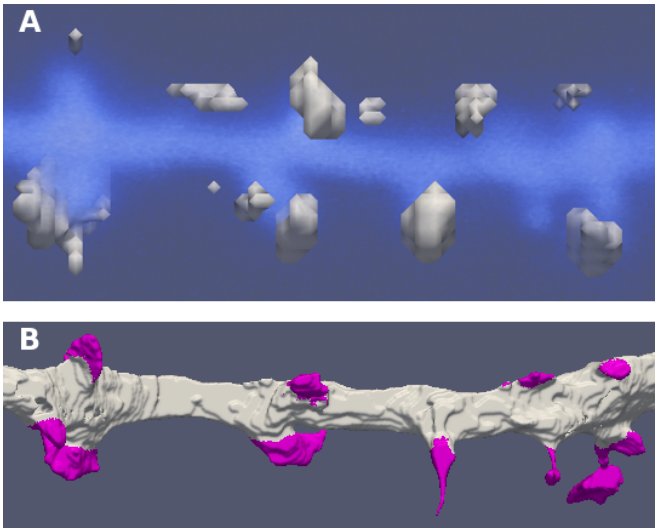

Fig. 7. A) Volume rendering of the fluorescence image and the surface reconstruction of the segmentation. B) Manual aligned reconstruction of the SBFS-EM data with highlighted spines (*pink*).

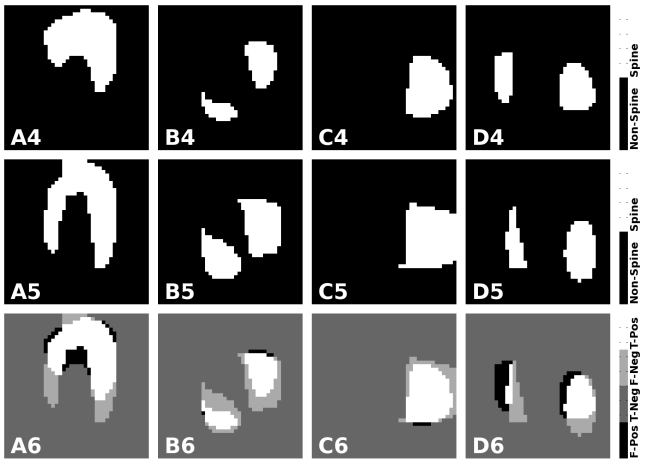

Fig. 6. Binarized results of prediction maps $s_{s,i}$ (*first row*) and of ground truth data $P_{s,i}$ (*second row*). The *third row* shows a comparison between correct (*dark gray* and *white*) and wrong (*light gray* and *black*) classified pixels.

dendrite like in the synthetic case but imaged with 2-photon microscopy. The backbone was approximated automatically (using a thinning algorithm) and 2D slices extracted. Then the model was applied to generate a prediction for these 2D images. The predictions of the 2D images were transformed back to the 3D space and then binarized with a manually selected threshold $t = 0.35$. Fig. 7 shows the results. The *first row* shows a volume rendering of the fluorescence image and in *grey* a surface reconstruction of the segmentation. The *second row* shows for the same piece of dendrite the reconstruction of the SBFS-EM data (spines are highlighted in *pink*). This direct comparison of the segmentation with the geometrically correct reconstruction is possible because of the correlative data set. The use of the same piece of dendrite in the synthetic and the real case shows that the approach can be transferred from synthetic data to real fluorescence images. The application to real fluorescence data shows the power of the supervised learning approach trained with synthetic data.

V. Conclusion

We presented a novel approach to compute 2D models for fluorescence data that uses *a-priori* knowledge from electron microscopy reconstructions. The information transfer from reconstructions to fluorescence images and the combined models enabled us to classify pixels of 2D slices orthogonal to the backbone into spine or non-spine.

The synthetic and real fluorescence examples illustrated how to model the distribution of fluorescence intensity from dendrites and spine probabilities in 2D thanks to DRFIs. Enough training data can easily be computed in 2D.

The process pipeline is working with real fluorescence images. Furthermore, by the use of a correlative data set it became possible to compare the results with the geometrical correct reconstruction of dendrite and spines. This showed also that the approach gives similar predictions for synthetic data and real fluorescence images.

Acknowledgments

This work was supported by an IPhD grant of the SystemsX.ch initiative evaluated by the Swiss National Science Foundation.

References

[1] Jie Cheng, Xiaobo Zhou, Eric Miller, Rochelle M. Witt, Jinmin Zhu, Bernardo L. Sabatini, and Steven T.C. Wong, "A novel computational approach for automatic dendrite spines detection in two-photon laser scan microscopy," *J. Neurosci. Mehtods*, vol. 165, no. 1, pp. 122–134, 2007.

[2] Firdaus Janoos, Kishore Mosaliganti, Xiaoyin Xu, Raghu Machiraju, Kun Huang, and Stephen T.C. Wong, "Robust 3d reconstruction and identification of dendritic spines from optical microscopy imaging," *Medical Image Analysis*, vol. 13, no. 1, pp. 167–179, 2009.

[3] Xiaosong Yuan, Joshua T. Trachtenberg, Steve M. Potter, and Badrinath Roysam, "Mdl constrained 3-d grayscale skeletonization algorithm for automated extraction of dendrites and spines from fluorescence confocal images," *Neuroinformatics*, vol. 7, no. 4, pp. 213–232, 2009.

[4] Yong Zhang, Xiaobo Zhou, Rochelle M. Witt, Bernardo L. Sabatini, Donald Adjeroh, and Stephen T.C. Wong, "Automated spine detection using curvilinear structure detector and lda classifier," in *Proc. of ISBI*, 2007, pp. 528–531.

[5] Wengang Zhou, Houqiang Li, and Xiaobo Zhou, "3d dendrite reconstruction and spine identification," in *Proc. of MICCAI*, 2008, pp. 18–26.

[6] Yong Zhang, Kun Chen, Matthew Baron, Merilee A. Teylan, Yong Kim, Zhihuan Song, Paul Greengard, and Stephen T.C. Wong, "A neurocomputational method for fully automated 3d dendritic spine detection and segmentation of medium-sized spiny neurons," *NeuroImage*, vol. 50, no. 4, pp. 1472–1484, 2010.

[7] Peng Shi, Xiaobo Zhou, Qing Li, Matthew Baron, Merilee A. Teylan, Yong Kim, and Stephen T.C. Wong, "Online three-dimensional dendritic spines morphological classification based on semi-supervised learning," in *Proc. of ISBI*, 2009, pp. 1019–1022.

[8] Alfredo Rodriguez, Douglas B. Ehlenberger, Dara L. Dickstein, Patrick R. Hof, and Susan L. Wearne, "Automated three-dimensional detection and shape classification of dendritic spines from fluorescence microscopy images," *PlosOne*, vol. 3, no. 4, 2007.

[9] Winfried Denk and Heinz Horstmann, "Serial block-face scanning electron microscopy to reconstruct three-dimensional tissue nanostructure," *PLoS Biol*, vol. 2, no. 11, pp. 1900–1909, 2004.

[10] Bo Zhang, Josiane Zerubia, and Jean-Christophe Olivo-Marin, "Gaussian approximations of fluorescence microscope psf models," *Applied Optics*, vol. 46, no. 10, pp. 1819–1829, 2007.

[11] Warren R. Zipfel, Rebecca M. Williams, and Watt W. Webb, "Nonlinear magic: multiphoton microscopy in the biosciences," *Nature Biotechnology*, vol. 21, no. 11, pp. 1369 – 1377, 2003.